

Light hyperclusters and hyperons in low-density hot stellar matter

Tiago Custódio, Helena Pais, and Constança Providência

CFisUC, Department of Physics, University of Coimbra, 3004-516 Coimbra, Portugal.

The abundance of light nuclei and hyperons, that are produced in stellar environments such as supernova or binary mergers, is calculated within a relativistic mean-field model with density dependent couplings in low-density matter. Five light nuclei are considered, together with three light hypernuclei. We show that the presence of hyperons shifts the dissolution of clusters to larger densities, and increases the amount of clusters. This effect is larger the smaller the charge fraction, and the higher the temperature. The abundance of hyperons is also affected by the cluster formation: neutral and positively charged hyperons suffer a reduction, and the negatively charged ones an increase. We also observe that the dissolution of the less-abundant clusters occurs at larger densities due to smaller Pauli-blocking effects. Overall, hypernuclei set in at temperatures above 25 MeV, and depending on the temperature and chemical composition, they may be more abundant than α -particles, or even more abundant than other heavier clusters.

I. INTRODUCTION

Light nuclei are found in core-collapse supernova matter and in binary neutron star (NS) mergers. Their presence may impact the evolution of these systems by affecting the rate at which the weak reactions take place during the core collapse [7, 8], or the dissolution of the remnant torus of accreted matter that is formed around the high mass NS after a binary merger [9]. Light clusters could also influence the dissipative processes that determine the post-merger evolution and mass ejection from the remnant [10, 11].

These clusters have been detected in heavy ion collisions in several experiments, such as ALICE at the Large Hadron Collider (LHC), STAR at the Relativistic Heavy Ion Collider (RHIC), or J-PARC, from the E13 collaboration. Some of these states, like the deuteron, the hypertriton [1], the hyper-hydrogen4 [2] or the hyperhelium4 [3] are loosely bound objects with quite a large radius. It is still not understood why these states are well described within a thermal approach with a temperature production of the order of 150 MeV, much larger than their binding energy [4]. At RHIC and LHC, the baryonic chemical potential is quite low. The formation of light clusters at much smaller temperatures, of the order of 5 to 12 MeV, but larger densities, below 0.1 fm^{-3} , has been measured by the multi-detectors NIMROD at the Texas A&M University [5] and INDRA [6] at GANIL. These last measurements can help understand the low-density nuclear matter equation of state (EoS) at temperatures and densities of interest to the evolution of supernovae and binary neutron star mergers.

Neutron stars are formed by cold catalysed β -equilibrium matter constituted by neutrons, protons, electrons and muons below a density $\approx 2n_0 - 3n_0$, where $n_0 \approx 0.15 \text{ fm}^{-3}$ is the saturation density of symmetric nuclear matter. At larger densities other degrees of freedom such as hyperons, deltas, kaon or pion condensates or quark matter may set in [12]. During the supernova or binary merger evolution, β -equilibrium is not necessarily achieved and temperatures as high as 50 to 100 MeV

may be attained. To describe these events, it is necessary, therefore, to consider a wide range of electron fractions, temperatures and densities. In Refs. [13, 14], it has been shown that the inclusion of the complete baryonic octet decreases the free energy of matter, and the EoS based on relativistic mean-field models, like DD2 [15] or SFHo [16], including the complete baryonic octet, have been built and made available in the CompOSE database [17]. In both of these studies, it was shown that, at low densities, the hyperons compete with light nuclear clusters, and the minimization of the free energy should allow for the appearance of hyperons at very low densities, which, however, was not implemented.

However, in the nineties, one could already find EoS with light clusters included, like the general-purpose EoS by Lattimer and Swesty [18], or the EoS by Shen *et al.* [19], based on the single-nucleus approximation. In both cases, light clusters were restricted to α -particles. Improved models of the non-homogeneous matter at finite temperature containing light clusters in the framework of nuclear statistical equilibrium were proposed later [20, 21]. In these models, the introduction of an excluded volume is necessary to dissolve the clusters at high densities. A different approach was undertaken in Refs. [15, 22, 23], where density effects are included within a relativistic mean-field approach that describes the light clusters as new particles which couple to the mesonic fields. The model, first published in Ref. [15], introduces the temperature-dependent cluster binding shifts determined from a quantum statistical approach to nuclear matter in thermodynamic equilibrium [24–27]. This model was recently improved, by taking into account continuum correlations, and it was applied to simulations of core-collapse supernovae [8]. In particular, the authors analysed the effect of medium modifications on the simulations.

In Ref. [32], the possible appearance of hyperons in the density region of the non-homogeneous matter that forms the inner crust of a neutron star was analyzed. Temperatures below the melting temperature of the heavy clusters that form this region were considered, i.e $T \lesssim 15 \text{ MeV}$. It was found that only very small amounts of hy-

perons, like Λ fractions below 10^{-5} , were present in the background gas. The low-density EoS of stellar matter including light clusters and heavy baryons was also studied in Ref. [33]. In addition to hyperons, the author also considered delta-baryons, pions, and the presence of a representative heavy cluster. It was shown that, depending on temperature and density, the composition of matter may shift from a greater abundance of light clusters to a heavy-baryon predominance.

In the present work, we are going to simultaneously calculate, in a consistent way, the abundance of light nuclei and hypernuclei, as well as hyperons, within the DD2 relativistic mean-field (RMF) model [15], taking for the σ -meson cluster coupling the value obtained in [31]. The introduction of light clusters is going to follow the approach first presented in Ref. [28], where the effect of the medium on the binding energy of the clusters is considered through the introduction of a binding energy shift, together with a universal coupling of the σ -meson to the different light clusters, that was chosen so that the equilibrium constants of the NIMROD experiment [5] were reproduced. In Refs. [29, 30], the same approach was applied to the description of the INDRA data [6] including the medium effects on the data analysis. It was verified that, in this case, the equilibrium constants could be reproduced only if a larger σ -meson coupling was introduced. The calibration of the σ -meson to the clusters coupling was later performed for other models in Ref. [31].

The paper is organized as follows: in Sec. II, we introduce the formalism, in Sec. III the results are presented for different scenarios: the effect of temperature, charge fraction, and density, and the inclusion of hyperons, light clusters and hyperclusters. Finally, in Sec. IV, some conclusions are drawn.

II. FORMALISM

In this section, we present the model used throughout the paper, and we discuss how hyperons, light clusters and light hyperclusters, which are considered as point-like particles, are included within our approach.

Our system's gas is constituted by unbound neutrons (n) and protons (p), as well the following six hyperons: Λ , Σ^- , Σ^0 , Σ^+ , Ξ^- , Ξ^0 . Together, these eight particles form the spin-1/2 baryonic octet.

Immersed in this gas, we will also consider five purely nucleonic light nuclei (${}^2\text{H}$, ${}^3\text{H}$, ${}^3\text{He}$, ${}^4\text{He}$, ${}^6\text{He}$) as well as three hypernuclei: the ${}^3_{\Lambda}\text{H}$ hypertriton, the ${}^4_{\Lambda}\text{H}$ hyperhydrogen4 and the hyperhelium4 ${}^4_{\Lambda}\text{He}$. For each of these three hypernuclei, a nucleon was replaced by a Λ hyperon. In Table I, the spin and isospin projection quantum numbers can be found for each particle considered here.

In the RMF theory, the interactions between different baryons are mediated by the exchange of virtual mesons. Here we will consider the following four mesons: the isoscalar-scalar σ meson field that provides the attractive

strong force; the isoscalar-vector ω^μ meson field responsible for the repulsive strong force; the isoscalar-vector ϕ^μ meson field responsible for an extra repulsion between two hyperons, and the isovector-vector ρ^μ meson field which accounts for the isospin dependence of the interactions. The baryons are described by a Dirac spinor.

The Lagrangian density for this system reads [12, 14, 15, 28]:

$$\mathcal{L} = \sum_{b=\text{baryonic octet}} \mathcal{L}_b + \sum_{i=\text{light nuclei}} \mathcal{L}_i + \sum_{j=\text{light hypernuclei}} \mathcal{L}_j + \sum_{m=\sigma,\omega,\phi,\rho} \mathcal{L}_m. \quad (1)$$

The subscript b stands for the eight particles belonging to the spin-1/2 baryonic octet ($n, p, \Lambda, \Sigma^-, \Sigma^0, \Sigma^+, \Xi^-, \Xi^0$).

A. The homogeneous gas

The Lagrangian density of the gas, which includes the spin-1/2 baryonic octet, is given by

$$\mathcal{L}_b = \bar{\Psi}_b [i\gamma_\mu \partial^\mu - m_b + g_{\sigma b} \sigma - g_{\omega b} \gamma_\mu \omega^\mu - g_{\rho b} \gamma_\mu \vec{I}_b \cdot \vec{\rho}^\mu - g_{\phi b} \gamma_\mu \phi^\mu] \Psi_b, \quad (2)$$

with Ψ_b the baryon field, and \vec{I}_b the isospin operator. The quantities g_{mb} are the coupling constants of the interactions between the baryons and the mesons.

We take for the vacuum proton and neutron mass an average value, $m = m_n = m_p = 939$ MeV. For the hyperons, we consider the following masses: $m_\Lambda = 1115.683$ MeV, $m_{\Sigma^-} = 1197$ MeV, $m_{\Sigma^0} = 1193$ MeV, $m_{\Sigma^+} = 1189$ MeV, $m_{\Xi^-} = 1321$ MeV, and $m_{\Xi^0} = 1315$ MeV.

The coupling constants g_{mN} of the nucleons ($N = n, p$) to the σ , ω and ρ mesons are given by the RMF model DD2 [15] with density-dependent coupling constants. These couplings are written in the form

$$g_{mN}(n_B) = g_{mN}(n_0) h_M(x), \quad x = n_B/n_0, \quad (3)$$

where the density n_B is the baryonic density. For the isoscalar couplings, the function h_M is given by [15],

$$h_M(x) = a_M \frac{1 + b_M(x + d_M)^2}{1 + c_M(x + d_M)^2} \quad (4)$$

and for the isovector couplings has the form

$$h_M(x) = \exp[-a_M(x - 1)]. \quad (5)$$

The values of the parameters a_M, b_M, c_M , and d_M are given in Ref. [15].

As for the hyperons ($\Lambda, \Sigma^-, \Sigma^0, \Sigma^+, \Xi^-, \Xi^0$), their coupling constants g_{mb} can be defined in terms of the nucleon couplings as $g_{mb} = R_{mb} g_{mN}$, for $m = \sigma, \omega, \rho$ and $g_{\phi b} = R_{\phi b} g_{\omega N}$. All these coupling constants of the mesons to the different hyperons, normalized to the respective meson nucleon coupling, can be found in Table II. In the case of the ϕ -meson, the coupling to the ω

TABLE I. Spin (J) and isospin projection (I_3) quantum numbers for all particles considered in our system.

	n	p	Λ	Σ^-	Σ^0	Σ^+	Ξ^-	Ξ^0	${}^2\text{H}$	${}^3\text{H}$	${}^3\text{He}$	${}^4\text{He}$	${}^6\text{He}$	${}^3_{\Lambda}\text{H}$	${}^4_{\Lambda}\text{H}$	${}^4_{\Lambda}\text{He}$
J	1/2	1/2	1/2	1/2	1/2	1/2	1/2	1/2	1	1/2	1/2	0	0	1/2	0	0
I_3	-1/2	1/2	0	-1	0	1	-1/2	1/2	0	-1/2	1/2	0	-1	0	-1/2	1/2

meson is used instead, because the nucleons do not couple to this meson (their coupling is zero, $g_{\phi N} = 0$). This is the “ideal mixing” scenario [34], where the hyperon couplings to the ω and ϕ mesons is fixed using the SU(6) quark model. For the hyperon couplings to the ρ meson, they are the same as for the nucleons. Concerning this coupling, what differentiates each hyperon is simply their isospin projection. This will also be true for all the clusters and hyperclusters considered in our model.

The coupling of the Λ hyperon to the σ meson can be calibrated by fitting the experimental binding energy of Λ hypernuclei as described in [14]. From Ref. [14], we chose to use the value of the DDME2D-a model, $R_{\sigma\Lambda} = 0.621$. Similarly, for the Ξ coupling to the σ meson, we use the calibrated value obtained in there, $R_{\sigma\Xi} = 0.320$ [35]. Finally, according to Ref. [36], the Σ potential in symmetric nuclear matter lies in the range $U_{\Sigma}^{(N)}(n_0) \approx 30 \pm 20$ MeV, so we fix $U_{\Sigma}^{(N)}(n_0) = 30$ MeV, and we obtain $g_{\sigma\Sigma} = 0.474$.

TABLE II. Coupling constants of the mesons to the different hyperons, normalized to the respective meson nucleon coupling, i.e. $R_{Mj} = g_{Mj}/g_{MN}$, except for the ϕ -meson. Here the $g_{\omega N}$ is used for normalisation.

b	$R_{\sigma b}$	$R_{\omega b}$	$R_{\phi b}$	$R_{\rho b}$
Λ	0.621	2/3	$-\sqrt{2}/3$	1
Σ	0.474	2/3	$-\sqrt{2}/3$	1
Ξ	0.320	1/3	$-2\sqrt{2}/3$	1

B. The light clusters

Following Refs. [28, 29], the Lagrangian density for the fermionic spin-1/2 light nuclei reads

$$\mathcal{L}_i = \bar{\Psi}_i [\gamma_{\mu} i D_i^{\mu} - M_i^*] \Psi_i, \quad i = {}^3\text{H}, {}^3\text{He}, \quad (6)$$

and for the bosonic light nuclei is given according to their spins,

$$\mathcal{L}_i = \frac{1}{2} (i D_i^{\mu} \Psi_i)^* (i D_{\mu} \Psi_i) - \frac{1}{2} \Psi_i^* (M_i^*)^2 \Psi_i, \quad i = {}^4\text{He}, {}^6\text{He}, \quad (7)$$

$$\mathcal{L}_i = \frac{1}{4} (i D_i^{\mu} \Psi_i^{\nu} - i D_i^{\nu} \Psi_i^{\mu})^* (i D_{\mu} \Psi_{\nu} - i D_{\nu} \Psi_{\mu}) - \frac{1}{2} \Psi_i^{\mu*} (M_i^*)^2 \Psi_{\mu}, \quad i = {}^2\text{H}, \quad (8)$$

with

$$i D_i^{\mu} = i \partial^{\mu} - g_{\omega i} \omega^{\mu} - g_{\rho i} \vec{I}_i \cdot \vec{\rho}^{\mu}. \quad (9)$$

$g_{\omega i}$ and $g_{\rho i}$ are the couplings of cluster i to the ω and ρ mesons, respectively. They are defined as $g_{\omega i} = A_i g_{\omega N}$, with A_i the cluster mass number, and $g_{\rho i} = g_{\rho N}$. The effective mass of the cluster i , M_i^* , is given by

$$M_i^* = A_i m - g_{\sigma i} \sigma - (B_i^0 + \delta B_i), \quad (10)$$

where $g_{\sigma i} = x_s A_i g_{\sigma N}$ is the σ -cluster coupling (x_s being the σ -cluster coupling fraction calibrated in [31]), B_i^0 is the tabulated vacuum binding energy of light cluster i and δB_i is the binding energy shift,

which was first defined in Ref. [28] as:

$$\delta B_i = \frac{Z_i}{n_0} (\epsilon_p^* - m n_p^*) + \frac{N_i}{n_0} (\epsilon_n^* - m n_n^*). \quad (11)$$

The total binding energy B_i is given by

$$B_i = A_i m^* - M_i^*, \quad i = {}^2\text{H}, {}^3\text{H}, {}^3\text{He}, {}^4\text{He}, {}^6\text{He}. \quad (12)$$

In the above expressions, Z_i , N_i are the number of protons and neutrons, respectively, and $m^* = m - g_{\sigma N} \sigma$ is the nucleon effective mass. The gas energy density ϵ_i^* and nucleonic density n_i^* , are given by

$$\epsilon_i^* = \frac{1}{\pi^2} \int_0^{p_{F_i}(\text{gas})} p^2 e_i(p) (f_{i+}(p) + f_{i-}(p)) dp \quad (13)$$

$$n_i^* = \frac{1}{\pi^2} \int_0^{p_{F_i}(\text{gas})} p^2 (f_{i+}(p) + f_{i-}(p)) dp, \quad (14)$$

where $p_{F_i}(\text{gas}) = (3\pi^2 n_i)^{1/3}$ is the Fermi momentum of nucleon i defined using the zero temperature relation between the density and the Fermi momentum, $f_{i\pm}$ are the usual Fermi distribution functions for the particles and anti-particles, and $e_i = \sqrt{p_i^2 + m^{*2}}$ is the corresponding single-particle energy of the nucleon i .

C. The light hyperclusters

The light hyperclusters are introduced in a similar way as the purely nucleonic light clusters. The Lagrangian density for the fermionic light hypercluster $j = {}^3_{\Lambda}\text{H}$ is given by:

$$\mathcal{L}_j = \bar{\Psi}_j [\gamma_{\mu} i D_j^{\mu} - M_j^*] \Psi_j, \quad j = {}^3_{\Lambda}\text{H}, \quad (15)$$

with

$$i D_j^{\mu} = i \partial^{\mu} - g_{\omega j} \omega^{\mu} - g_{\phi j} \phi^{\mu}, \quad (16)$$

whereas for the bosonic light hyperclusters, $j = {}^4_{\Lambda}\text{H}, {}^4_{\Lambda}\text{He}$, the Lagrangian density is given by

$$\mathcal{L}_j = \frac{1}{2} (iD_j^\mu \Psi_j)^* (iD_{\mu j} \Psi_j) \quad (17)$$

$$-\frac{1}{2} \Psi_j^* (M_j^*)^2 \Psi_j, \quad j = {}^4_{\Lambda}\text{H}, {}^4_{\Lambda}\text{He},$$

with

$$iD_j^\mu = i\partial^\mu - g_{\omega j} \omega^\mu - g_{\phi j} \phi^\mu - g_{\rho j} \vec{I}_j \cdot \vec{\rho}^\mu. \quad (18)$$

The coupling of the hyperclusters to the ω meson is defined as

$$g_{\omega j} = (A_j - 1)g_{\omega N} + g_{\omega \Lambda}, \quad (19)$$

and the coupling to the ϕ meson is the same as the one of the Λ -hyperon coupling, $g_{\phi j} = g_{\phi \Lambda}$ ("ideal mixing" case). The coupling to the ρ -meson is the same as the coupling to the nucleons, $g_{\rho j} = g_{\rho N}$.

Following Eq.(10), the effective mass of the hypercluster j is given by

$$M_j^* = (A_j - 1)m + m_\Lambda - g_{\sigma j} \sigma - (B_j^0 + \delta B_j) \quad (20)$$

with

$$g_{\sigma j} = x_s((A_j - 1)g_{\sigma N} + g_{\sigma \Lambda}) \quad (21)$$

the σ -hypercluster coupling. Let M_j be the vacuum mass of a hypercluster j

$$M_j = (A_j - 1)m + m_\Lambda - B_j^0. \quad (22)$$

The vacuum masses for the hypertriton, ${}^3_{\Lambda}\text{H}$, the hyperhydrogen4, ${}^4_{\Lambda}\text{H}$, and the hyperhelium4, ${}^4_{\Lambda}\text{He}$, were obtained from [1],[2],[3], respectively: $M_{{}^3_{\Lambda}\text{H}} = 2990.89$ MeV, $M_{{}^4_{\Lambda}\text{H}} = 3922.49$ MeV, $M_{{}^4_{\Lambda}\text{He}} = 3921.70$ MeV. From Eq. (22), the vacuum binding energies can be extracted, $B_{{}^3_{\Lambda}\text{H}}^0 = 2.793$ MeV, $B_{{}^4_{\Lambda}\text{H}}^0 = 10.198$ MeV, and $B_{{}^4_{\Lambda}\text{He}}^0 = 10.981$ MeV.

From [37] we see that the experimental production ratio between ${}^3_{\Lambda}\text{H}$ and ${}^3\text{H}$ (${}^3_{\Lambda}\text{H}/{}^3\text{H}$) is 0.75 ± 0.07 . Since this ratio must be proportional to the square of the interaction $((g_{\sigma^3_{\Lambda}\text{H}}/g_{\sigma^3\text{H}})^2 \sim 0.76)$, we conclude that the way we define the σ -hypercluster couplings is in good accordance with experimental data.

Following the same procedure for the hyperclusters, their binding energy shift is given by

$$\delta B_j = \frac{Z_j}{n_0} (\epsilon_p^* - mn_p^*) + \frac{N_j}{n_0} (\epsilon_n^* - mn_n^*) + \frac{\Lambda_j}{n_0} (\epsilon_\Lambda^* - m_\Lambda n_\Lambda^*), \quad (23)$$

where Λ_j is the number of Λ hyperons present at each hypercluster j , which, for the present hyperclusters we consider, is always equal to 1. The energy density ϵ_Λ^* and the density n_Λ^* are similar to Eqs. (13) and (14), respectively, and the total binding energy for each hypercluster j , B_j is given by

$$B_j = (A_j - 1)m^* + m_\Lambda^* - M_j^*. \quad (24)$$

D. The mesonic fields

The Lagrangian density for the fields have the standard RMF expressions:

$$\mathcal{L}_\sigma = \frac{1}{2} \partial_\mu \sigma \partial^\mu \sigma - \frac{1}{2} m_\sigma^2 \sigma^2, \quad (25)$$

$$\mathcal{L}_\omega = -\frac{1}{4} \Omega^{\mu\nu} \Omega_{\mu\nu} + \frac{1}{2} m_\omega^2 \omega_\mu \omega^\mu, \quad (26)$$

$$\mathcal{L}_\phi = -\frac{1}{4} P^{\mu\nu} P_{\mu\nu} + \frac{1}{2} m_\phi^2 \phi_\mu \phi^\mu, \quad (27)$$

$$\mathcal{L}_\rho = -\frac{1}{4} \vec{R}^{\mu\nu} \cdot \vec{R}_{\mu\nu} + \frac{1}{2} m_\rho^2 \vec{\rho}_\mu \cdot \vec{\rho}^\mu, \quad (28)$$

with $\Omega_{\mu\nu} = \partial_\mu \omega_\nu - \partial_\nu \omega_\mu$, $P_{\mu\nu} = \partial_\mu \phi_\nu - \partial_\nu \phi_\mu$, and $\vec{R}_{\mu\nu} = \partial_\mu \vec{\rho}_\nu - \partial_\nu \vec{\rho}_\mu + g_\rho (\vec{\rho}_\mu \times \vec{\rho}_\nu)$.

We treat the binding energy shifts, δB_i , as in [15]: we replace the density dependence of these quantities by a vector meson dependence. This is equivalent, in our present study, to consider in the shifts δB_i the neutron, proton, and Λ densities replaced by

$$n_n = \frac{m_\omega^2}{2g_{\omega N}} \omega_0 - \frac{g_{\omega \Lambda}}{g_{\phi \Lambda}} \frac{m_\phi^2}{2g_{\omega N}} \phi_0 - \frac{m_\rho^2}{g_{\rho N}} \rho_{03}, \quad (29)$$

$$n_p = \frac{m_\omega^2}{2g_{\omega N}} \omega_0 - \frac{g_{\omega \Lambda}}{g_{\phi \Lambda}} \frac{m_\phi^2}{2g_{\omega N}} \phi_0 + \frac{m_\rho^2}{g_{\rho N}} \rho_{03}, \quad (30)$$

$$n_\Lambda = \frac{m_\phi^2}{g_{\phi \Lambda}} \phi_0. \quad (31)$$

With the inclusion of the binding energy shift for each cluster and hypercluster, the equations for the fields read:

$$m_\sigma^2 \sigma = \sum_b g_{\sigma b} n_b^s + \sum_i g_{\sigma i} n_i^s + \sum_j g_{\sigma j} n_j^s, \quad (32)$$

$$m_\rho^2 \rho_{03} = g_{\rho N} \left[\sum_b I_{3b} n_b + \sum_i I_{3i} n_i + \sum_j I_{3j} n_j \right] \quad (33)$$

$$- \frac{m_\rho^2}{g_{\rho N} n_0} \left(-\frac{\partial \epsilon_n^*}{\partial n_n} + \frac{m \partial n_n^*}{\partial n_n} \right) (n_{^3\text{H}}^s + 2n_{^3\text{He}}^s + n_{^4\text{H}}^s)$$

$$- \frac{m_\rho^2}{g_{\rho N} n_0} \left(\frac{\partial \epsilon_p^*}{\partial n_p} - \frac{m \partial n_p^*}{\partial n_p} \right) (n_{^3\text{He}}^s + n_{^4\text{He}}^s)$$

$$- \frac{m_\rho^2}{g_{\rho N} n_0} \left(-\frac{\partial \epsilon_n^*}{\partial n_n} + \frac{m \partial n_n^*}{\partial n_n} + \frac{\partial \epsilon_p^*}{\partial n_p} - \frac{m \partial n_p^*}{\partial n_p} \right)$$

$$\times \left(\sum_i n_i^s + \sum_j n_j^s \right),$$

$$\begin{aligned}
m_\omega^2 \omega_0 &= \sum_b g_{\omega b} n_b + \sum_i g_{\omega i} n_i + \sum_j g_{\omega j} n_j \quad (34) \\
&- \frac{m_\omega^2}{2g_{\omega N} n_0} \left(\frac{\partial \epsilon_n^*}{\partial n_n} - \frac{m \partial n_n^*}{\partial n_n} \right) (n_{^3\text{H}}^s + 2n_{^6\text{He}}^s + n_{^4\text{H}}^s) \\
&- \frac{m_\omega^2}{2g_{\omega N} n_0} \left(\frac{\partial \epsilon_p^*}{\partial n_p} - \frac{m \partial n_p^*}{\partial n_p} \right) (n_{^3\text{He}}^s + n_{^4\text{He}}^s) \\
&- \frac{m_\omega^2}{2g_{\omega N} n_0} \left(\frac{\partial \epsilon_n^*}{\partial n_n} - \frac{m \partial n_n^*}{\partial n_n} + \frac{\partial \epsilon_p^*}{\partial n_p} - \frac{m \partial n_p^*}{\partial n_p} \right) \\
&\times \left(\sum_i n_i^s + \sum_j n_j^s \right),
\end{aligned}$$

$$\begin{aligned}
m_\phi^2 \phi_0 &= \sum_{\substack{b=\Lambda, \Sigma^{-,0,+}, \\ \Xi^{-,0}}} g_{\phi b} n_b + \sum_j g_{\phi j} n_j \quad (35) \\
&+ \frac{g_{\omega\Lambda} m_\phi^2}{2g_{\omega N} g_{\phi\Lambda} n_0} \left(\frac{\partial \epsilon_n^*}{\partial n_n} - \frac{m \partial n_n^*}{\partial n_n} \right) (n_{^3\text{H}}^s + 2n_{^6\text{He}}^s + n_{^4\text{H}}^s) \\
&+ \frac{g_{\omega\Lambda} m_\phi^2}{2g_{\omega N} g_{\phi\Lambda} n_0} \left(\frac{\partial \epsilon_p^*}{\partial n_p} - \frac{m \partial n_p^*}{\partial n_p} \right) (n_{^3\text{He}}^s + n_{^4\text{He}}^s) \\
&- \frac{m_\phi^2}{g_{\phi\Lambda} n_0} \left(\frac{\partial \epsilon_\Lambda^*}{\partial n_\Lambda} - \frac{m_\Lambda \partial n_\Lambda^*}{\partial n_\Lambda} \right) (n_{^3\text{H}}^s + n_{^4\text{H}}^s + n_{^4\text{He}}^s) \\
&+ \frac{g_{\omega\Lambda} m_\phi^2}{2g_{\omega N} g_{\phi\Lambda} n_0} \left(\frac{\partial \epsilon_n^*}{\partial n_n} - \frac{m \partial n_n^*}{\partial n_n} + \frac{\partial \epsilon_p^*}{\partial n_p} - \frac{m \partial n_p^*}{\partial n_p} \right) \\
&\times \left(\sum_i n_i^s + \sum_j n_j^s \right),
\end{aligned}$$

where I_{3b} , I_{3i} , I_{3j} correspond to the isospin projections of the baryons b , light clusters i and light hyperclusters j , respectively. The quantities n_b , n_i , n_j correspond to the particle's densities, whereas n_b^s , n_i^s , n_j^s represent their scalar densities.

E. Chemical Equilibrium

In our system, the charge fraction Y_Q is fixed and defined as:

$$Y_Q = \sum_b q_b Y_b + \sum_i \frac{q_i}{A_i} Y_i + \sum_j \frac{q_j}{A_j} Y_j \quad (36)$$

where q_b , q_i , q_j are the electric charges of baryon b , light cluster i and light hypercluster j , respectively. The quantities Y_b , Y_i and Y_j correspond to the mass fractions of the different particles and are given by:

$$Y_b = \frac{n_b}{n_B}, \quad Y_i = A_i \frac{n_i}{n_B}, \quad Y_j = A_j \frac{n_j}{n_B}, \quad (37)$$

where n_B is the total density of the system.

The chemical potential μ_b of baryon b can be written as:

$$\mu_b = \mu_n - q_b \mu_e \quad (38)$$

where μ_n , μ_e are the neutron and electrical charge chemical potentials, respectively. Since $\mu_e = \mu_n - \mu_p$, the hyperon chemical potentials can be written in terms of the nucleons chemical potentials: $\mu_\Lambda = \mu_n$, $\mu_{\Sigma^-} = 2\mu_n - \mu_p$, $\mu_{\Sigma^0} = \mu_n$, $\mu_{\Sigma^+} = \mu_p$, $\mu_{\Xi^-} = 2\mu_n - \mu_p$, $\mu_{\Sigma^0} = \mu_n$.

For a light cluster i , their chemical potential μ_i can also be defined as a function of μ_n and μ_p :

$$\mu_i = N_i \mu_n + Z_i \mu_p \quad (39)$$

whereas for a light hypercluster j , μ_Λ also needs to be taken into account:

$$\mu_j = N_j \mu_n + Z_j \mu_p + \Lambda_j \mu_\Lambda. \quad (40)$$

The effective chemical potential μ_c^* of any particle $c = b, i, j$ present in our system can be written in terms of its chemical potential μ_c as:

$$\mu_c^* = \mu_c - g_{\omega c} \omega_0 - g_{\phi c} \phi_0 - g_{\rho c} I_{3c} \rho_{03} - A_c \Sigma_0^R \quad (41)$$

where Σ_0^R is the rearrangement term present in models with density-dependent couplings in order to guarantee thermodynamical consistency:

$$\begin{aligned}
\Sigma_0^R &= \sum_c \left(\frac{\partial g_{\omega c}}{\partial n_B} \omega_0 n_c + \frac{\partial g_{\phi c}}{\partial n_B} \phi_0 n_c + I_{3c} \frac{\partial g_{\rho c}}{\partial n_B} \rho_{03} n_c \right. \\
&\quad \left. - \frac{\partial g_{\sigma c}}{\partial n_B} \sigma_0 n_c^s \right). \quad (42)
\end{aligned}$$

III. RESULTS

In the present section we discuss how the presence of light clusters affects the abundances of heavy baryons at low densities and temperatures $T \lesssim 50$ MeV, and two different charge fractions, $Y_Q = 0.1$ and 0.3 . Above the critical temperature, $T_c \approx 15$ MeV, we do not expect the presence of heavy clusters, so, and as mentioned in the previous Sections, we consider 5 light clusters, ^2H , ^3H , ^3He , ^4He and ^6He , which were measured by INDRA [6], and three light hypernuclei $^3_\Lambda\text{H}$, $^4_\Lambda\text{H}$, $^4_\Lambda\text{He}$. All the calculations shown are for the DD2 RMF model [15]. In Ref. [31], the cluster-meson σ coupling fraction x_s was calibrated to the equilibrium constants obtained in [6] for different RMF models. For the density-dependent DD2 RMF model, a value of $x_s = 0.93 \pm 0.02$ was obtained. This range of values is going to be used throughout this work.

In Fig. 1, we plot the mass fractions of light clusters (^2H , ^3H , ^3He , ^4He and ^6He) and unbound protons and neutrons in equilibrium as a function of density for two temperatures $T = 10$ MeV (top) and 30 MeV (bottom) and two different values of the charge fraction $Y_Q = 0.3$

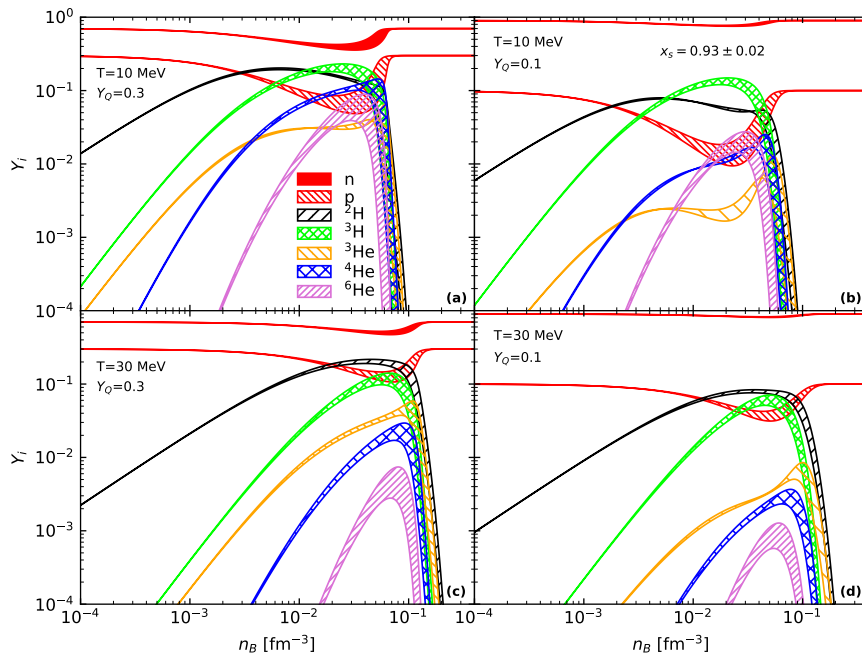


FIG. 1. Mass fractions of light clusters (${}^2\text{H}$, ${}^3\text{H}$, ${}^3\text{He}$, ${}^4\text{He}$ and ${}^6\text{He}$) and unbound protons and neutrons in equilibrium are plotted versus the density for $T = 10$ MeV (top) and 30 MeV (bottom) with charge fraction of $Y_Q = 0.3$ (left) and 0.1 (right). The bands take into account the uncertainty on the x_s coupling fraction of the clusters to the σ -meson.

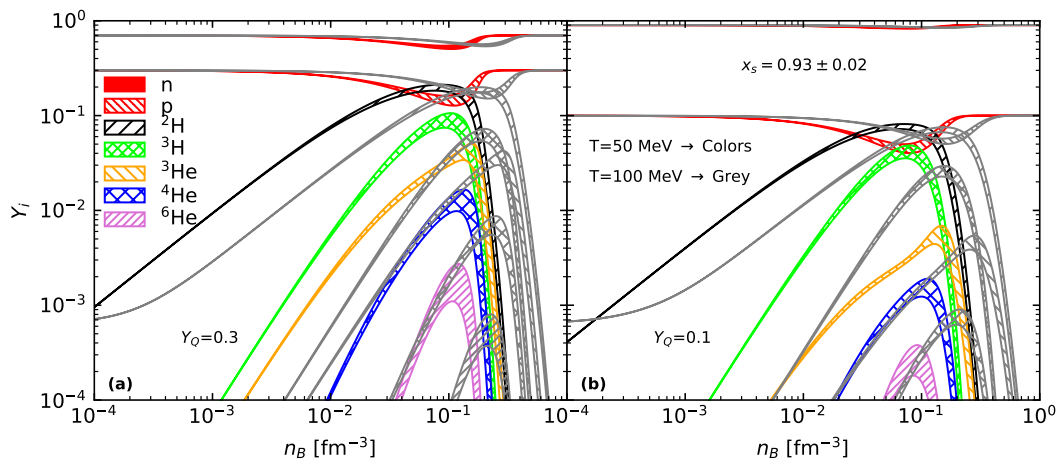


FIG. 2. Mass fractions of light clusters (${}^2\text{H}$, ${}^3\text{H}$, ${}^3\text{He}$, ${}^4\text{He}$ and ${}^6\text{He}$) and unbound protons and neutrons in equilibrium are plotted versus the density for $T = 50$ MeV (colored lines) and 100 MeV (grey lines), with a charge fraction of $Y_Q = 0.3$ (left) and 0.1 (right). The bands take into account the uncertainty on the x_s coupling fraction of the clusters to the σ -meson.

(left) and 0.1 (right). The bands take into account the uncertainty on x_s , and mainly affect the fraction maximum and the dissolution density. Several comments are in order concerning the effect of the temperature and charge: i) at the lowest densities, it is the mass that de-

termines the most abundant light cluster, and the smaller the mass the larger the abundance; ii) for $T = 10$ MeV, the most abundant cluster at the fraction maximum is the tritium, reflecting the isospin asymmetry. In particular, ${}^6\text{He}$ becomes more abundant than ${}^3\text{He}$ for the

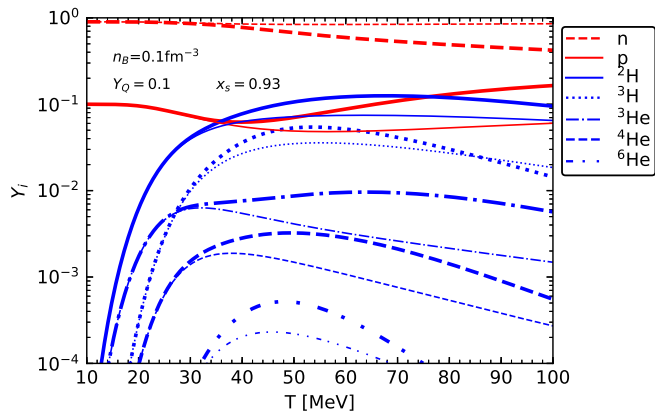


FIG. 3. Unbound nucleon and light cluster fractions in a calculation with (thick lines) and without (thin lines) hyperons as a function of the temperature for a charge fraction of $Y_Q = 0.1$, and a density of $n_B = 0.1 \text{ fm}^{-3}$. The scalar cluster-meson coupling is fixed to $x_s = 0.93$.

two charge fractions considered; iii) at $T = 30 \text{ MeV}$, the mass defines the largest abundances; iv) for $T = 10 \text{ MeV}$, it is interesting to observe that even though ${}^3\text{He}$ is less abundant than ${}^3\text{H}$, ${}^4\text{He}$ or ${}^6\text{He}$, it dissolves at larger densities. This is an effect of the binding energy shift that depends on the density of unbound neutrons and protons separately. The neutrons, being more abundant, have a stronger effect, and, in particular, affect more the clusters with a larger neutron fraction; v) for large temperatures, here represented by $T = 30 \text{ MeV}$, the deuteron is the most abundant for all densities due to its smaller mass. Moreover, at the maximum of the cluster fractions, their mass fractions are larger than the proton fraction.

In Fig. 2, the mass fractions are again plotted against the density, but this time for two larger temperatures, $T = 50$ and 100 MeV , the last one represented by grey lines to be well distinguished from the $T = 50 \text{ MeV}$ case. As already discussed for $T = 30 \text{ MeV}$, the relative abundances of the light nuclei are dictated by their masses, the deuteron being the most abundant and ${}^6\text{He}$ the least. The superposition of the distribution for both temperatures shows clearly that an increase of the temperature pushes the light-nuclei maxima to larger densities and reduces the abundances of the heavier clusters: only the deuteron keeps a similar fraction at the maximum. The cluster dissolution shifts to much larger densities for the larger temperature. A reduction of the charge fraction reduces the cluster fractions: for $T = 100 \text{ MeV}$, $Y_Q = 0.1$ the fraction of ${}^6\text{He}$ is always below 10^{-4} .

In order to better understand the effect of the temperature, we show in Fig. 3 the unbound nucleon and cluster abundances as a function of the temperature for a charge fraction $Y_Q = 0.1$ and a density $n_B = 0.1 \text{ fm}^{-3}$. This density value was chosen because it is where the fraction of the clusters is close to a maximum in the range of temperatures considered. It is seen that the abundance

of deuterons surpasses the one of protons for $25 \lesssim T \lesssim 70 \text{ MeV}$. It is also above $T = 25 \text{ MeV}$ that the cluster fractions obtained with and without hyperons start differing, and they start being more abundant in the presence of hyperons.

The effect of the inclusion of light clusters on the hyperon fractions is clearly seen in Fig. 4: the thick lines were obtained including clusters, while the calculation without clusters is represented by thin lines. The main effect of introducing clusters is a reduction of the unbound nucleons and of the electrically neutral or positive hyperons, while the fraction of the negatively charged hyperons increases. The formation of clusters is energetically favored but these clusters are positively charged, so its formation is compensated by a reduction of the unbound nucleons, together with a reduction (increase) of positively (negatively) charged baryons. A decrease of the neutron fraction also induces a reduction of the other neutral baryons. Moreover, a smaller charge fraction favors the formation of negatively charged baryons, and for $Y_Q = 0.1$, it is seen a clear competition between Σ^- and Λ for the smaller densities. At smaller densities, for a fixed temperature, the hyperon mass defines the abundance, but for larger densities, the magnitude and sign of the hyperon potential is reflected on the hyperon abundances. In particular, the fraction of Ξ^- s which feels an attractive potential becomes larger than the one of Σ^- which feels a repulsive interaction.

The effect of the hyperons on the cluster abundances, which was already seen in Fig. 3, and on the dissolution densities is clearly seen in Fig. 5. In the left panel, we show the total mass fraction of all the light clusters at $T = 50 \text{ MeV}$ (notice the linear scale on the x-axis contrary to the log-scale used in the previous figures), and in the right panel, the dissolution density of the clusters, n_d , which was defined as the density for which the cluster fraction has dropped to 10^{-4} is displayed. The charge fraction is set to $Y_Q = 0.3$ and 0.1 , and the scalar cluster-meson coupling fraction to $x_s = 0.93$. Two different calculations are compared: a calculation with the full baryonic octet (solid lines), and excluding hyperons (dashed lines). The main effects of including hyperons are: i) to increase the cluster fraction above the maximum of the cluster distribution, shifting the dissolution density to larger densities, the larger the temperature the stronger the effect; ii) the increase of the dissolution density starts to be non-negligible for $T \gtrsim 25 - 30 \text{ MeV}$; iii) the smaller the charge fraction, the stronger the effect. For $T = 50 \text{ MeV}$, the main effect is an increase of the dissolution density of the order of 10% if $Y_Q = 0.3$, and 20% for $Y_Q = 0.1$. Since the presence of the hyperons reduces the nucleon fraction, this is reflected on the medium effects felt by the clusters through the binding energy shift that is smaller. Moreover, the couplings to mesons become smaller since the couplings of the hyperons to the mesons are weaker. This explains why the effect of the hyperons on the clusters is larger for $Y_Q = 0.1$, since, as we saw in Fig. 4, a smaller charge fraction corresponds

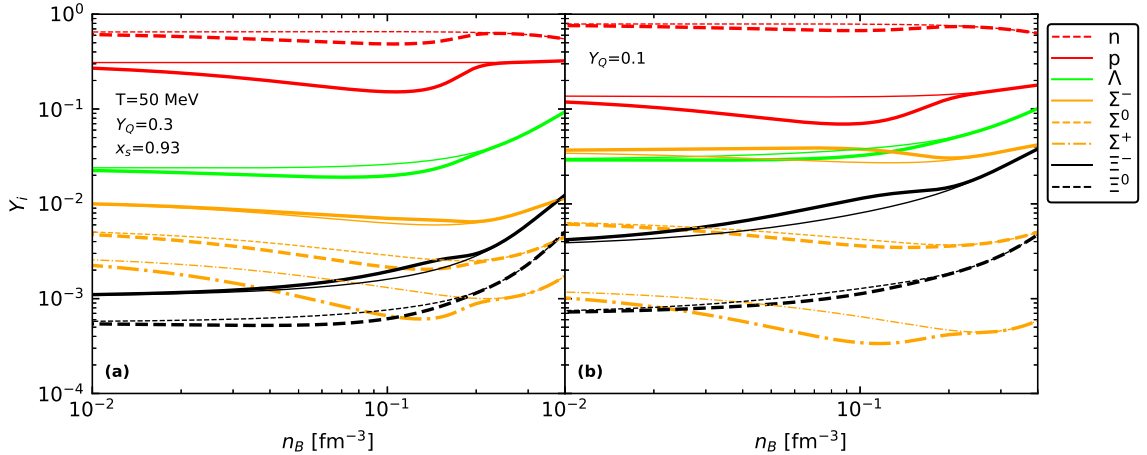


FIG. 4. Unbound nucleon and hyperon fractions as a function of the density in a calculation with (thick lines) and without (thin lines) light clusters, for a charge fraction of $Y_Q = 0.3$ (left) and 0.1 (right) and $T = 50$ MeV. The scalar cluster-meson coupling fraction is set to $x_s = 0.93$.

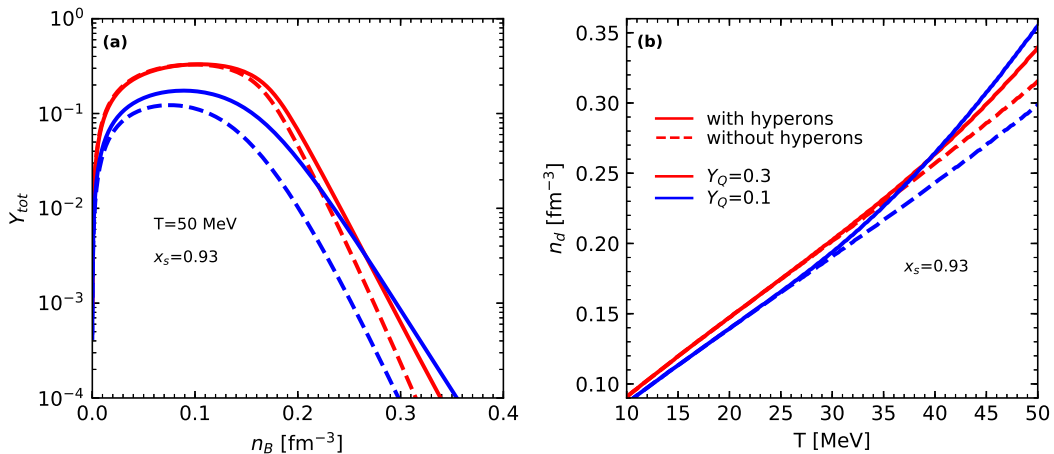


FIG. 5. Total mass fraction of the light clusters as a function of the density at $T = 50$ MeV (left) and the dissolution density of the clusters, n_d , as a function of the temperature (right) for a calculation with (solid) and without (dashed) hyperons and a charge fraction of $Y_Q = 0.3$ (red) and 0.1 (blue). The scalar cluster-meson coupling fraction is set to $x_s = 0.93$.

to an overall larger hyperon fraction.

In the following figures, we are going to study the effect of considering hyperclusters in our calculations. As mentioned in the previous sections, we take ${}^3_{\Lambda}\text{H}$, known as hypertriton, ${}^4_{\Lambda}\text{H}$ (hyperhydrogen 4), and ${}^4_{\Lambda}\text{He}$ (hyperhelium 4).

A fraction of hypernuclei above 10^{-4} is only obtained for big enough temperatures, i.e. $T \gtrsim 25$ MeV; for lower temperatures, the abundance of Λ hyperons is still too small to give rise to significant hypercluster fractions. Therefore, in the next two Figures, we consider $T = 50$ MeV. In Fig. 6, the light nuclei and hypernuclei mass fractions are plotted together with the unbound proton and neutron fractions, the Λ fraction, the total Σ frac-

tion corresponding to the sum of the $\Sigma^{+,0,-}$ fractions, and the total Ξ fraction corresponding to the sum of the $\Xi^{0,-}$ fractions, for a charge fraction of $Y_Q = 0.3$ (left) and 0.1 (right). There is a clear competition between the hypernuclei and the ${}^4\text{He}$ and ${}^6\text{He}$ light clusters, i.e. the light clusters with a larger mass: for $Y_Q = 0.1$, the hypernuclei have larger abundances, but even for the larger charge fraction, the dissolution density occurs at larger densities for the hypernuclei. The behavior of the hyperclusters in the medium is defined by their couplings to the mesons. The difference in relation to the light clusters may be attributed to the fact that hypernuclei are interacting more weakly with the medium, which is clearly seen considering the hypercluster couplings defined in Eqs. (19) and

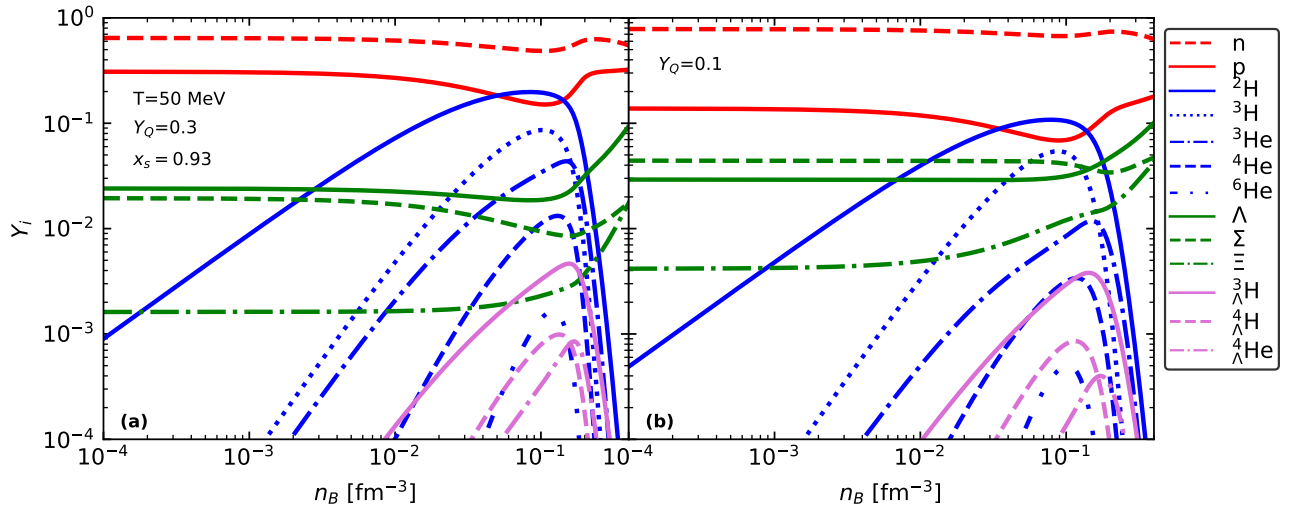


FIG. 6. Mass fractions of the unbound protons and neutrons (red lines), Λ , Σ and Ξ (green lines), light clusters (blue lines) and light hypernuclei (pink lines) as a function of the density for $T = 50$ MeV and $x_s = 0.93$, with $Y_Q = 0.3$ (left) and 0.1 (right).

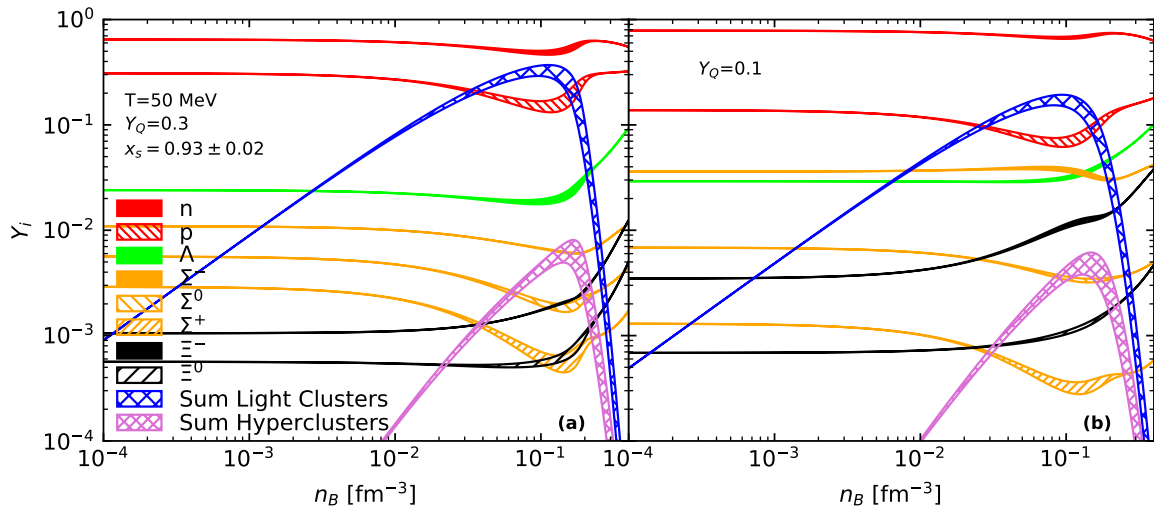


FIG. 7. Mass fractions of the unbound protons and neutrons (red), Λ (green), $\Sigma^{-,0,+}$ (orange) and $\Xi^{-,0}$ (black), total light clusters (blue) and light hypernuclei (pink) as a function of the density for $T = 50$ MeV and $x_s = 0.93 \pm 0.02$, with $Y_Q = 0.3$ (left) and 0.1 (right).

(21). Since the coupling of the hyperclusters to the ω -meson is strongly correlated with the dissolution density, a smaller ω -coupling implies larger dissolution densities. On the other hand, a weaker coupling to the σ -meson gives rise to smaller mass fractions, since a smaller binding occurs. Also, the binding energy shift is weaker for the hypernuclei: this binding shift is introduced to take into account Pauli blocking, but hypernuclei have less nucleons and therefore experience smaller shifts.

It is also interesting to notice that the isospin pair formed by the hyperclusters ${}^4_{\Lambda}\text{H}$ and ${}^4_{\Lambda}\text{He}$ behaves in a

similar way to the analogous isospin pair formed by the purely nucleonic clusters ${}^3\text{H}$ and ${}^3\text{He}$. In fact, since the Λ -hyperon present at the hyperclusters has isospin zero, the interactions of these two pairs of clusters with the medium is similar, the only difference being their masses and binding energies, resulting in smaller fractions for the hyperclusters.

In Fig. 7, the total light cluster fraction and the total light hypercluster fraction are compared with the baryonic octet fractions for the two charge fractions, 0.3 and 0.1 . We take $T = 50$ MeV, and we calculate the ef-

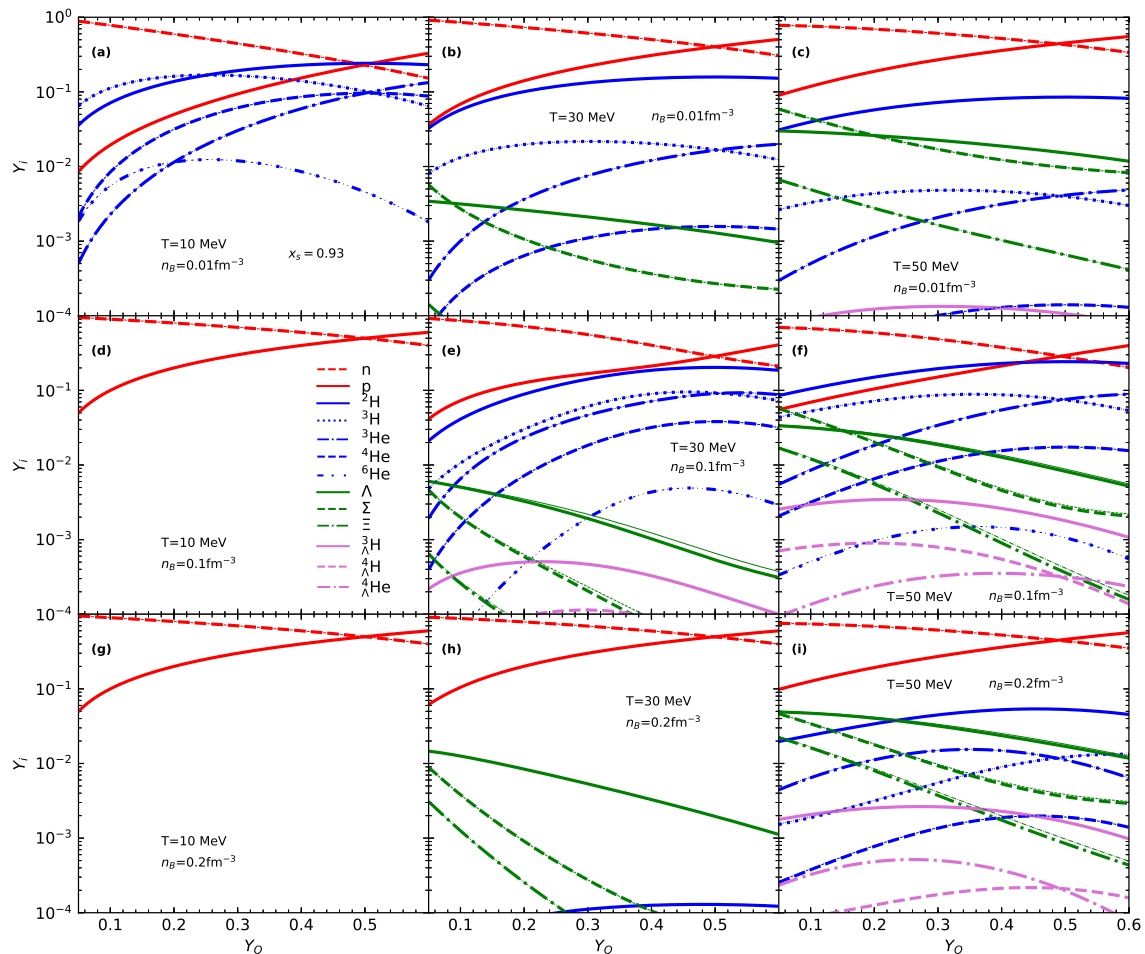


FIG. 8. Mass fractions of the unbound protons and neutrons (red), unbound hyperons: Λ (solid green), sum of $\Sigma^{+,0,-}$ (dashed green) and sum of $\Xi^{-,0}$ (dash-dotted green), light clusters (blue), and light hypernuclei (pink) as a function of the charge fraction for $T = 10$ MeV (left), $T = 30$ MeV (middle) and $T = 50$ MeV (right). The fractions were determined at $n_B = 0.01$ fm^{-3} (top), 0.1 fm^{-3} (middle) and 0.2 fm^{-3} (bottom). The scalar cluster-meson coupling is set to $x_s = 0.93$.

fect of the uncertainty on the x_s coupling of the particle fractions, shown by the bands. The abundances of the hypernuclei are small compared to the light nuclei, and even taking $T = 100$ MeV (not shown), there is not a big difference whether the hypernuclei are included or not in the calculation, only slightly affecting the abundances of the heavier clusters and their dissolution density.

In order to understand how the charge fraction affects the light cluster abundances, and under which conditions the hyperclusters are more abundant, in Fig. 8, we plot for a fixed density (0.01 , 0.1 and 0.2 fm^{-3}), and temperatures 10 , 30 and 50 MeV, the cluster fractions as a function of the charge fraction. The densities chosen are

below, close and above the cluster fraction maxima. Depending on the temperature, the last two density values may be above the dissolution density, taken as the density for which the cluster fraction is below 10^{-4} . Considering the lowest density, we conclude that: i) for the lowest temperature, the most abundant clusters are not only determined by their mass, but also by their isospin and binding energy, contrary to the other two temperatures, for which the mass essentially determines their abundances, and only in a second order, the isospin; ii) hyperons are only present at $T = 30$ and 50 MeV, and hypernuclei appear with an abundance above 10^{-4} at $T = 30$ MeV for $n_B = 0.1$ fm^{-3} and at $T = 50$ MeV for

all densities considered; iii) protons may be less abundant than some light clusters, as for instance ${}^2\text{H}$ and ${}^3\text{H}$, below $Y_Q < 0.5$ for $T = 10$ MeV, and $T = 50$ MeV and $n_B = 0.1 \text{ fm}^{-3}$; iv) only for $T = 50$ MeV do hyperons become more abundant than most of the light clusters (only ${}^2\text{H}$ are more abundant). For $T = 10$ MeV and the lowest density, only nucleons are present, clusters have already dissolved and hyperons did not set in. For $T = 30$ MeV, at $n_B = 0.2 \text{ fm}^{-3}$, only deuterons did not dissolve and hypernuclei are only present for 0.1 fm^{-3} . For $T = 50$ MeV, hypernuclei are present in the three densities considered although only quite a few for the lowest density. Once again, a similar behaviour is observed for the pairs ${}^4_{\Lambda}\text{H}$, ${}^4_{\Lambda}\text{He}$ and ${}^3\text{H}$, ${}^3\text{He}$. Hypernuclei seem to be most abundant for charge fractions of the order of $Y_Q = 0.3$ in all situations studied.

IV. CONCLUSIONS

The effect of hyperonic degrees of freedom on the low-density EoS of hot matter, as may occur in events connected with neutron stars, was studied within the density-dependent DD2 RMF model. The study was performed at a fixed charge fraction and considered temperatures until 100 MeV. The degrees of freedom included in the calculations were nucleons, hyperons, and light nuclei and hypernuclei. The introduction of light clusters was done following the formalism first described in Ref. [28]. Light clusters couple to the mesonic fields and a binding energy shift is included in order to account for the Pauli blocking. This contribution essentially influences the dissolution density of the cluster. A similar formalism has been presented and applied in [8, 15, 38], the difference being the model description of the coupling of light clusters to the mesonic degrees of freedom. Moreover, in Ref. [15], the cluster binding shifts are temperature dependent, with the shifts determined from a quantum statistical calculation [26].

At low temperatures, the abundances are determined by the cluster binding energy and isospin, and for charge fractions below 0.3, light clusters like ${}^6\text{He}$ are more abundant than ${}^3\text{He}$ or even α -particles. However, neutron-rich clusters dissolve at lower densities due to the stronger binding energy shifts, which take into account Pauli

blocking effects. Larger temperatures shift the cluster fraction maxima and dissolution densities to larger densities, they decrease their abundances, except for the deuteron, and they define the cluster abundances in terms of their masses, with the light clusters being more abundant.

In this work, we also showed that the presence of hyperons shifts the dissolution of clusters to larger densities and increases the cluster abundances for temperatures $T \gtrsim 25$ MeV. This effect is larger the smaller the charge fraction, and the higher the temperature. The increase of clusters is attributed to a weaker effect of the Pauli-blocking implemented in the model via the binding energy shifts since the overall nucleon densities is lower. Besides, the clusters also affect the hyperon fractions: while neutral and positively charged baryons decrease when clusters are included, the fraction of negatively charged hyperons increase. Hypernuclei set in at temperatures above 25 MeV, and for $T \gtrsim 50$ MeV, they compete with α -particles and ${}^6\text{He}$. However, switching off the hypernuclei does not influence much the other particles. It was shown that the larger abundances for the total fraction of hyperclusters occurs for a charge fraction close to 0.3. One expects that a reduction of unbound nuclei and neutral or positively charged hyperons, and an increase of light clusters, will affect the reaction rates that determine the core-collapse supernova evolution or the binary merger.

In our model, clusters survive up to quite large densities if the temperatures are high. This must be further investigated and it may be necessary to include a temperature dependence on the binding energy shifts. Although one would expect that clusters would dissolve, it is also true that light clusters survive up to temperatures as high as 150 MeV as discussed in Ref. [4].

ACKNOWLEDGMENTS

This work was partly supported by the FCT (Portugal) Projects No. UID/FIS/04564/2020 and POCI-01-0145-FEDER-029912, and by PHAROS COST Action CA16214. H.P. acknowledges the grant CEECIND/03092/2017 (FCT, Portugal).

-
- [1] J. Adam *et al.* (STAR), *Nature Phys.* **16**, 409 (2020), arXiv:1904.10520 [hep-ex].
 [2] A. Esser, S. Nagao, F. Schulz, P. Achenbach, C. Ayerbe Gayoso, R. Böhm, O. Borodina, D. Bosnar, V. Bozkurt, L. Debenjak, M. O. Distler, I. Frišćić, Y. Fujii, T. Gogami, O. Hashimoto, S. Hirose, H. Kanda, M. Kaneta, E. Kim, Y. Kohl, J. Kusaka, A. Margaryan, H. Merkel, M. Mihovilović, U. Müller, S. N. Nakamura, J. Pochodzalla, C. Rappold, J. Reinhold, T. R. Saito, A. Sanchez Lorente, S. Sánchez Majos, B. S. Schlimme,

- M. Scoth, C. Sienti, S. Širca, L. Tang, M. Thiel, K. Tsukada, A. Weber, and K. Yoshida (A1 Collaboration), *Phys. Rev. Lett.* **114**, 232501 (2015).
 [3] T. O. Yamamoto, M. Agnello, Y. Akazawa, N. Amano, K. Aoki, E. Botta, N. Chiga, H. Ekawa, P. Ev-toukhovitch, A. Feliciello, M. Fujita, T. Gogami, S. Hasegawa, S. H. Hayakawa, T. Hayakawa, R. Honda, K. Hosomi, S. H. Hwang, N. Ichige, Y. Ichikawa, M. Ikeda, K. Imai, S. Ishimoto, S. Kanatsuki, M. H. Kim, S. H. Kim, S. Kinbara, T. Koike, J. Y. Lee,

- S. Marcello, K. Miwa, T. Moon, T. Nagae, S. Nagao, Y. Nakada, M. Nakagawa, Y. Ogura, A. Sakaguchi, H. Sako, Y. Sasaki, S. Sato, T. Shiozaki, K. Shirotori, H. Sugimura, S. Suto, S. Suzuki, T. Takahashi, H. Tamura, K. Tanabe, K. Tanida, Z. Tsamalaidze, M. Ukai, Y. Yamamoto, and S. B. Yang (J-PARC E13 Collaboration), *Phys. Rev. Lett.* **115**, 222501 (2015).
- [4] P. Braun-Munzinger and B. Dönigus, *Nucl. Phys. A* **987**, 144 (2019), arXiv:1809.04681 [nucl-ex].
- [5] L. Qin *et al.*, *Phys. Rev. Lett.* **108**, 172701 (2012), arXiv:1110.3345 [nucl-ex].
- [6] R. Bougault *et al.*, *J. Phys. G* **47**, 025103 (2020), arXiv:1911.08355 [nucl-ex].
- [7] A. Arcones, G. Martínez-Pinedo, E. O'Connor, A. Schwenk, H. T. Janka, C. J. Horowitz, and K. Langanke, *Phys. Rev. C* **78**, 015806 (2008), arXiv:0805.3752 [astro-ph].
- [8] T. Fischer, S. Typel, G. Röpke, N.-U. F. Bastian, and G. Martínez-Pinedo, *Phys. Rev. C* **102**, 055807 (2020), arXiv:2008.13608 [astro-ph.HE].
- [9] S. Rosswog, *Int. J. Mod. Phys. D* **24**, 1530012 (2015), arXiv:1501.02081 [astro-ph.HE].
- [10] M. G. Alford, L. Bovard, M. Hanauske, L. Rezzolla, and K. Schwenzer, *Phys. Rev. Lett.* **120**, 041101 (2018), arXiv:1707.09475 [gr-qc].
- [11] S. Fujibayashi, K. Kiuchi, N. Nishimura, Y. Sekiguchi, and M. Shibata, *Astrophys. J.* **860**, 64 (2018), arXiv:1711.02093 [astro-ph.HE].
- [12] N. K. Glendenning, *Compact Stars: Nuclear Physics, Particle Physics, and General Relativity (Astron. Astrophys. Library)* (Springer, 2000).
- [13] M. Marques, M. Oertel, M. Hempel, and J. Novak, *Phys. Rev. C* **96**, 045806 (2017), arXiv:1706.02913 [nucl-th].
- [14] M. Fortin, M. Oertel, and C. Providência, *Publ. Astron. Soc. Austral.* **35**, 44 (2018), arXiv:1711.09427 [astro-ph.HE].
- [15] S. Typel, G. Ropke, T. Klahn, D. Blaschke, and H. H. Wolter, *Phys. Rev. C* **81**, 015803 (2010), arXiv:0908.2344 [nucl-th].
- [16] A. W. Steiner, M. Hempel, and T. Fischer, *Astrophys. J.* **774**, 17 (2013), arXiv:1207.2184 [astro-ph.SR].
- [17] [Urlhttps://compose.obspm.fr/](https://compose.obspm.fr/).
- [18] J. M. Lattimer and F. D. Swesty, *Nucl. Phys. A* **535**, 331 (1991).
- [19] H. Shen, H. Toki, K. Oyamatsu, and K. Sumiyoshi, *Nucl. Phys. A* **637**, 435 (1998), arXiv:nucl-th/9805035.
- [20] M. Hempel and J. Schaffner-Bielich, *Nucl. Phys. A* **837**, 210 (2010), arXiv:0911.4073 [nucl-th].
- [21] A. R. Raduta and F. Gulminelli, *Phys. Rev. C* **82**, 065801 (2010), arXiv:1009.2226 [nucl-th].
- [22] S. S. Avancini, C. C. Barros, Jr., D. P. Menezes, and C. Providência, *Phys. Rev. C* **82**, 025808 (2010), arXiv:1007.2319 [nucl-th].
- [23] M. Ferreira and C. Providência, *Phys. Rev. C* **85**, 055811 (2012), arXiv:1206.0139 [nucl-th].
- [24] G. Ropke, *Phys. Rev. C* **79**, 014002 (2009), arXiv:0810.4645 [nucl-th].
- [25] G. Ropke, *Nucl. Phys. A* **867**, 66 (2011), arXiv:1101.4685 [nucl-th].
- [26] G. Röpke, *Phys. Rev. C* **92**, 054001 (2015), arXiv:1411.4593 [nucl-th].
- [27] G. Röpke, *Phys. Rev. C* **101**, 064310 (2020), arXiv:2004.09773 [nucl-th].
- [28] H. Pais, F. Gulminelli, C. Providência, and G. Röpke, *Phys. Rev. C* **97**, 045805 (2018), arXiv:1804.01328 [nucl-th].
- [29] H. Pais *et al.*, *Phys. Rev. Lett.* **125**, 012701 (2020), arXiv:1911.10849 [nucl-th].
- [30] H. Pais *et al.*, *J. Phys. G* **47**, 105204 (2020), arXiv:2006.07256 [nucl-th].
- [31] T. Custódio, A. Falcão, H. Pais, C. Providência, F. Gulminelli, and G. Röpke, *Eur. Phys. J. A* **56**, 295 (2020), arXiv:2009.14035 [nucl-th].
- [32] D. P. Menezes and C. Providência, *Phys. Rev. C* **96**, 045803 (2017), arXiv:1707.01338 [nucl-th].
- [33] A. Sedrakian, *Eur. Phys. J. A* **56**, 258 (2020), arXiv:2009.00357 [nucl-th].
- [34] S. Weissenborn, D. Chatterjee, and J. Schaffner-Bielich, *Phys. Rev. C* **85**, 065802 (2012), [Erratum: *Phys. Rev. C* **90**, 019904 (2014)], arXiv:1112.0234 [astro-ph.HE].
- [35] M. Fortin, A. R. Raduta, S. Avancini, and C. Providência, *Phys. Rev. D* **101**, 034017 (2020), arXiv:2001.08036 [hep-ph].
- [36] A. Gal, E. V. Hungerford, and D. J. Millener, *Rev. Mod. Phys.* **88**, 035004 (2016), arXiv:1605.00557 [nucl-th].
- [37] Z.-L. She, G. Chen, D.-M. Zhou, L. Zheng, Y.-L. Xie, and H.-G. Xu, *Phys. Rev. C* **103**, 014906 (2021), arXiv:2009.05402 [nucl-th].
- [38] M. Hempel, K. Hagel, J. Natowitz, G. Röpke, and S. Typel, *Phys. Rev. C* **91**, 045805 (2015), arXiv:1503.00518 [nucl-th].